ISSN 2176-5480

22nd International Congress of Mechanical Engineering (COBEM 2013)
November 3-7, 2013, Ribeirão Preto, SP, Brazil

BIPARAMETIC ANALYSIS OF THE ESCAPE DYNAMICS IN THE SOLAR SYSTEM: SOME PRELIMINARY RESULTS

Sheila Crisley de Assis
Maisa de Oliveira Terra
Instituto Tecnológico de Aeronáutica - ITA - Departamento de Matemática, São José dos Campos, SP, Brasil
sheassis@yahoo.com.br
maisa@ita.br

Abstract. *In this contribution we investigate the trajectory escape dynamics in some three-body subsystems of the Solar System, namely, Jupiter-Europa, Sun-Neptune and Pluto-Charon systems, considering a region of initial conditions near the smaller primary and considering the mathematical model given by the planar circular restricted three-body problem. Our main aim is to examine the properties of the four considered escape basins and the fractal properties of their boundaries. Modern mission strategies have exploit the use of many-body natural dynamics to design transfer orbits from the vicinity of a primary body to another region. Our analyses is valuable to identify the biparametric dependence of safe domains of the phase space which allow transfers to a specific region of interest, avoiding the effect of final state uncertainty with initial condition variations, that is, far from fractal basin boundaries. The two parameters considered here are the mass parameter of the mathematical model and the scaled mean radius of the smaller primary. Remarkably, both the size of the considered basins and the fractality of their boundaries depend strongly on the considered parameters. The spatial distribution of escape time values are also investigated and associated with the fractality of the boundaries.*

Keywords: *escape trajectories; Solar system; space mission design; fractal basin boundaries*

1. INTRODUCTION

An open Hamiltonian system or a Hamiltonian system with exits (Aguirre *et al.*, 2009) corresponds to the case at which a particle can escape toward infinity (or to another region of the phase space) from a certain bounded region, called the *scattering region*, for values of energy higher than a critical value, the escape energy. Since there are no attractors for Hamiltonian systems, we cannot define basins of attraction. However, we can define an exit basin in an analogous way to the basins of attraction. The exit basin associated with the exit k of an open Hamiltonian system is defined as the set of initial conditions that leaves the scattering region through exit k. The analysis of escape basins and their boundaries is of fundamental importance in the study of mass transport between regions of the phase space. Open Hamiltonian systems have been investigated in different contexts (Aguirre *et al.*, 2009; Bleher *et al.*, 1988). Moreover, a leaking of trajectories in a system produces relevant dynamical effects. In particular, in many problems of celestial mechanics and cosmology, many mathematical models consider gravitational interactions among bodies that are assumed to be punctual masses. If trajectories are extracted from the dynamics when they collide with the mean radius of these bodies, a leaking is formed around the center of these large bodies and a collisional basin can be considered.

The restricted three-body problem (RTBP) has been studied for years since Euler (1772) and Jacobi (1832), presenting a renewed interest nowadays. This mathematical model investigates the behavior of a third body under gravitational influence of two heavy primaries (Szebehely, 1967). Indeed, the analysis of escape processes of this system is relevant in many contexts of celestial mechanics, astrodynamics and astronautics, and can be applied to investigate transport processes of trajectories, both in the context of space mission design (Gómez *et al.*, 2004; Koon *et al.*, 2000; Sousa-Silva and Terra, 2012a,b) and on the study of dynamical evolution of natural systems, involving comets, asteroids and satellites. In particular, Assis and Terra (2013) explored in detail the escape basin dynamics in the planar restricted three-body problem with initial condition sets around the smaller primary for several values of C, while Saturnian subsystems have been investigated by Davis and Howell (2011, 2012) over short-term and medium-term integrations.

This contribution aims to investigate the processes of escape of trajectories in the context of the planar circular restricted three-body problem for three different subsystems of the Solar system, considering the scattering region around the smaller primary. For each system, we adopted a value of C below and near C_2, because this corresponds to a region very important for transfer orbit design in modern space mission. We verify a strong dependence of the properties of escape basins and their boundaries with respect to two parameters, namely, the scaled mean radius of the smaller primary and the mass parameter of the model.

This paper is organized as follows. In Section 2, we present the considered dynamical model; while in Section 3, the definitions adopted for the escape basin analysis are stated. Numerical results of escape basins, Poincaré sections and escape time analysis are explored in Section 4. Section 5 presents the conclusions.

ISSN 2176-5480

2. DESCRIPTION OF THE MATHEMATICAL MODEL

The planar circular restricted three-body problem (PCR3BP) (Szebehely, 1967) describes the motion of a third body P_3 moving in the gravitational field of two bodies, P_1 and P_2, called primaries. Usually, this third body represents a spacecraft or a natural body, as an asteroid or a satellite. As the mass of the third body is much smaller than the masses of the primaries, it is assumed that the motion of P_1 and P_2 is not perturbed by P_3, being a solution of a two-body $(2B)$ problem. In the circular version of the model, the orbits of P_1 and P_2 are coplanar circles centered in the barycenter of this $2B$ system and, in the planar version of the model, the motion of P_3 is restricted to the plane of motion of the primaries. The dimensionless mass parameter of the model is defined as $\mu = m_2/(m_1 + m_2)$, with $m_1 > m_2$, while the masses of P_1 and P_2 are given, respectively, by $1 - \mu$ and μ.

The spacecraft's equations of motion are given by

$$\ddot{x} - 2\dot{y} = \Omega_x \qquad \text{and} \qquad \ddot{y} + 2\dot{x} = \Omega_y \tag{1}$$

with

$$\Omega(x, y) = \frac{x^2 + y^2}{2} + \frac{1 - \mu}{r_1} + \frac{\mu}{r_2} + \frac{\mu(1 - \mu)}{2}, \tag{2}$$

$$r_1 = \left[(x + \mu)^2 + y^2\right]^{\frac{1}{2}} \qquad \text{and} \qquad r_2 = \left[(x + 1 - \mu)^2 + y^2\right]^{\frac{1}{2}}. \tag{3}$$

This system has an integral of motion J, known as the *Jacobi Constant*, and that is given by

$$J(x, y, \dot{x}, \dot{y}) = 2\Omega(x, y) - (\dot{x}^2 + \dot{y}^2) = C. \tag{4}$$

The conservation associated to J restricts the motion in the four-dimensional phase space to a three-dimensional invariant manifold. The Jacobi constant C is related with the third body's energy E by $C = -2E$, given that, as usual,

$$E(x, y, \dot{x}, \dot{y}) = \frac{1}{2}(\dot{x}^2 + \dot{y}^2) + \Omega(x, y). \tag{5}$$

2.1 Lagrangian Points

This dynamical model has five equilibria defined by

$$\frac{\partial J}{\partial x} = \Omega_x = 0, \qquad \frac{\partial J}{\partial y} = \Omega_y = 0, \qquad \frac{\partial J}{\partial \dot{x}} = 0 \Rightarrow \dot{x} = 0, \qquad \frac{\partial J}{\partial \dot{y}} = 0 \Rightarrow \dot{y} = 0. \tag{6}$$

These equilibria are called Lagrangian points, being:

- Three collinear points, namely L_1 , L_2 and L_3, localized in the x-axis (saddle-center solutions).
- Two triangular points, called L_4 and L_5, localized in the vertices of equilateral triangle (center-center solutions).

The Jacobi constant values at L_k are denoted by C_k.

2.2 Accessible Regions

The conservation associated to J defines a three-dimensional invariant manifold in the four-dimensional phase space

$$M(\mu, C) = \left\{(x, y, \dot{x}, \dot{y}) \in \mathbb{R}^4 | J(x, y, \dot{x}, \dot{y}) = C\right\}. \tag{7}$$

The accessible regions to the trajectories for a given value of C can be obtained by the projection of the surface ***M*** in the space of positions *(x, y)* and imposing the constrain $\dot{x}^2 + \dot{y}^2 = 2\Omega(x, y) - C \geq 0$. These regions are called *Hill Regions* and are given by

$$\mathcal{M}(\mu, C) = \{(x, y) | \Omega(x, y) \geq C/2\}. \tag{8}$$

The boundaries of these regions are the called *zero-velocity curves* (zvc), since they are the locus in the $x - y$ plane, where kinetic energy vanishes. It is easy to verify that there are five possible cases for the Hill's regions, defined by the C_k values, as is shown Fig. 1.

ISSN 2176-5480

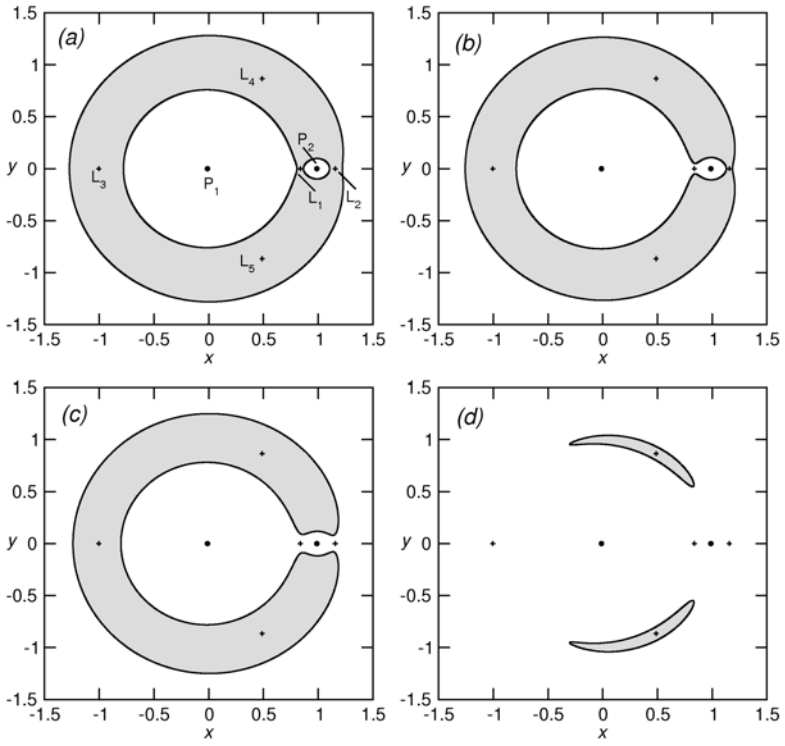

Figure 1. The five cases of the possible Hill's regions. The white regions represent the Hill's regions, while the dark regions correspond to the inaccessible ones. In Case 1, $C > C_1$, no transfer orbit between the primaries is possible. In Case 2, $C_1 > C > C_2$ there are only internal transfers, while in Case 3 ($C_2 > C > C_3$) and Case 4 ($C_3 > C > C_4 = C_5$), internal and external connections are possible. The fifth case is not shown, and it corresponds to $C < C_4 = C_5$. In Case 5, all the plane is accessible.

3. ESCAPE BASINS

In this contribution, we perform a biparametric analysis of the process of escape of trajectories in the planar circular restricted three-body problem, considering three different subsystems of the Solar system. The two considered parameters are the usual mass parameter μ of the mathematical model and the scaled mean radius of the smaller primary defined by

$$R_H = \frac{R_{P_2}}{d_{P_1 P_2}} \left(\frac{3}{\mu}\right)^{1/3}, \tag{9}$$

where R_{P_2} denotes the mean radius of the smaller primary and $d_{P_1 P_2}$ denotes the distance between the two primaries.

The initial condition sets are defined around the smaller primary, more precisely between the Lagrangian collinear points L_1 and L_2. This constitutes the called *scattering region*. As we are adopting values of C between C_1 and C_2, trajectories can have four different behaviors, defining four possible escape basins: *the bounded basin* constituted by trajectories that remain in the scattering region until the the maximum time integration t_f, *the larger primary basin* of trajectories which exit through L_1 before t_f, *the exterior basin* of trajectories which exit through L_2 before t_f, and *the collisional basin* of trajectories which collide with the smaller primary surface before t_f and before escape from the scattering region. These basins are represented by the colors green, blue, red and black, respectively. All the results of escape basins were obtained with the fixed value of 200 dimensionless time unit (dtu) for t_f, which was enough to provide a good representation of the steady-state solutions for the considered cases.

Thus, to build escape diagrams in a three-dimensional manifold of fixed C, we consider a uniform grid of about 1600×1300 initial conditions in the Poincaré section S defined in the (x, y) plane for $\dot{x} = 0$ and $\dot{y} > 0$, for $x_{L_1} \leq x \leq x_{L_2}$, where x_{L_k} denotes the x coordinate of L_k, $k = 1, 2$, and $y_i \leq y \leq y_f$, with the values of y_i and y_f varying with to the adopted system.

As we will see, the long escape time values are associated with fractals basin boundaries and stickiness effect. According to Contopoulos and Harsoula (2008, 2010), the stickiness effect happens when in a nonhyperbolic or mixed Hamiltonian system, the last KAM curve is destroyed with an increasing of the perturbation (here increasing the energy or decreasing C) and a cantorus is formed. Cantorus are fractal Cantor sets containing an infinite number of gaps, which allows the communication of the inner chaotic domain with the outer chaotic sea. However, for a energy value above the

ISSN 2176-5480

critical value associated with this phenomenon, transport through the cantorus takes a very long time and, so, these fractal sets act as a partial barrier to local chaotic diffusion. So, sticky orbits stay for a long time in certain regions of phase space, producing a distinct distribution of points in chaotic zones.

4. ESCAPE DYNAMICS RESULTS

In this section, we investigate the escape dynamics, presenting escape basin diagrams and plots of the spatial distributions of escape time values of specific basins for the three considered systems, i.e., Sun-Neptune, Pluto-Charon, and Jupiter-Europe, for a value of C near and below the respective C_2 value of each case, that is, a value of C immediately after the opening of the neck around the Lagrangian point L_2. This C region is of central interest, both in the point of view of dynamical system and of practical applications, in particular, for transfer orbit design in modern space missions and in the investigation of temporary capture of comets and asteroids around of the smaller primary. These subsystems were selected because they illustrate three qualitative distinct regimes we observed, inspecting several cases in the Solar System. Besides escape results, the qualitative investigation of the dynamics is performed through Poincaré sections in order to elucidate the obtained results.

4.1 SUN-NEPTUNE SYSTEM

Initially, we investigate the Sun-Neptune system with mass parameter $\mu = 5.146971254 \times 10^{-5}$ and $R_H = 2.1318 \times 10^{-4}$ (a low μ and low R_H case). In this case, 200 dtu corresponds to $5,254.8$ years. Figure 2 presents the Poincaré section S and the escape basin diagram for $C = 3.005795$, while Fig. 3 shows the diagram of each one of the four escape basins separately.

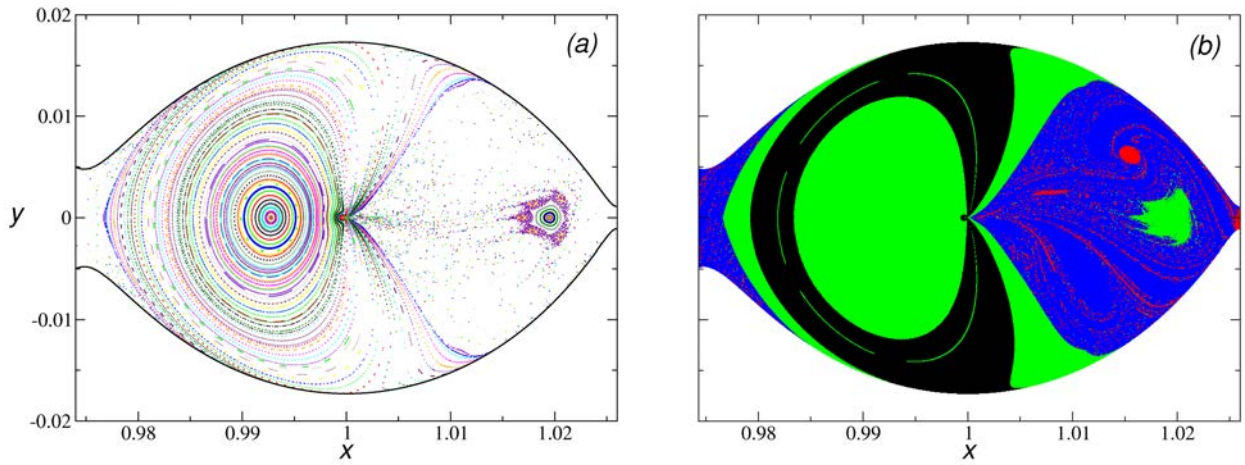

Figure 2. Results for Sun-Neptune system for $C = 3.005795$. **a** Poincaré section S and **b** basin diagram for $t_f = 200$ dtu, with bounded basin (green), collisional set (black), larger primary basin (blue) and exterior basin (red).

A large region of regular motion is found at the left side of the small primary in the Poincaré section S, while a small stability island, surrounded by remarkable sticky motion, is seen immersed in a large chaotic sea at the right side of S. We remark that all these solutions, in general, correspond to trajectories around the primary, but traveled in opposite sense. Given the choice of the sign of $\dot{y}$ for the definition of S, at the left side of S, we observe mainly the quasiperiodic orbits traveled in the clockwise sense around the small primary (hence, retrograde in relation to the rotating coordinate system), besides a small portion of chaotic trajectories. On the other hand, at the right side of S, both chaotic and quasiperiodic motions traveled in anticlockwise sense are seen (direct in relation to the rotating coordinate system). Concerning the escape basin diagram, many interesting aspects can be noted. For this system and C, the collisional basin presents a smooth boundary, contains 36% of the total considered initial conditions and is absolutely absent of the chaotic sea regions, as we can observe comparing Figs. 2a, 2b and 3b. This last fact implies that all escape solutions are far from unsafe solutions for this energy level. As expected, the bounded basin appears in the quasiperiodic motion regions of the Poincaré section S. The sparse bounded solutions seen in the chaotic sea region indicate that the maximum integration time was not enough to provide the final state of some long time escape solutions. For this t_f value, the bounded basin contains 24% of the total initial conditions analyzed. Increasing t_f, one must observe the escape of the sparse solutions along the chaotic sea for medium escape time, while higher escape time values must correspond to the sticky trajectories which are seen surrounding the stability island at the right side of S. Figure 3 (c) and (d) contain the two escaping basins through the channels of the two Lagrangian equilibria.

Comparing them, we verify that the boundary between these two basins can be both smooth and fractal, more precisely,

ISSN 2176-5480

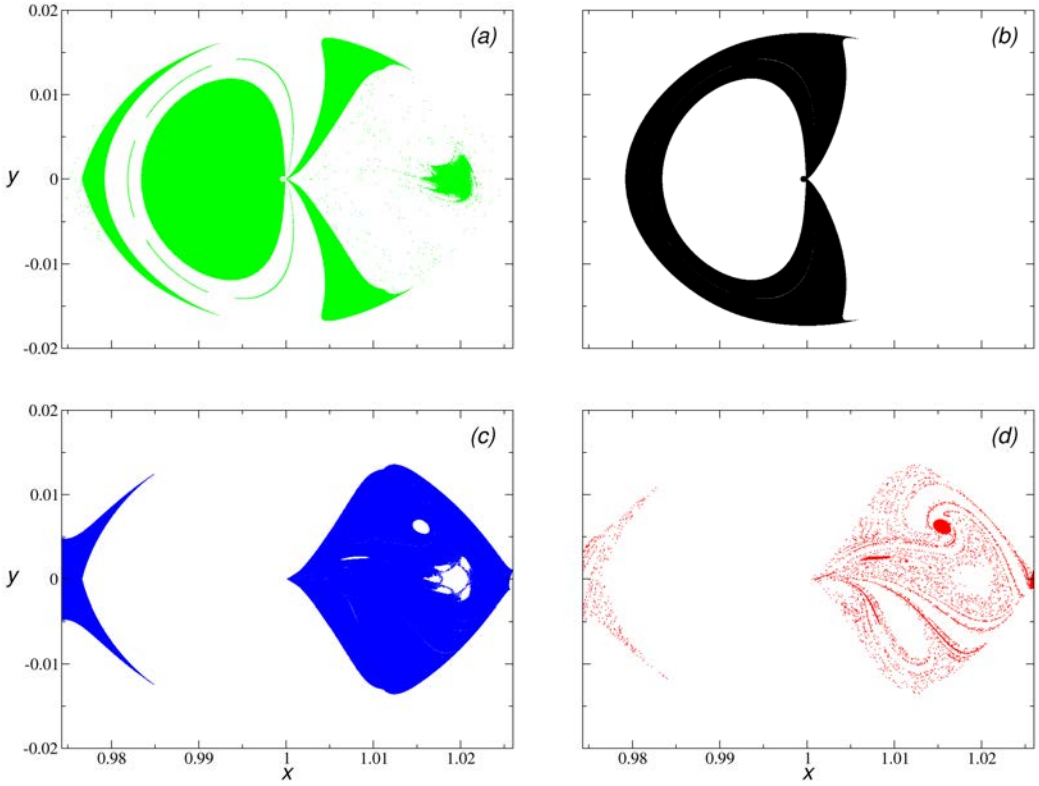

Figure 3. Detail of the escape basin diagram for Sun-Neptune system for $C = 3.005795$ and $t_f = 200$ dtu, presenting **a** the bounded basin (green), **b** the collisional basin (black), **c** the larger primary basin (blue) and **d** the exterior basin (red).

smooth portions of the boundary correspond to the first six or seven cuts of the stable manifold of the Lyapunov periodic orbit around L_2, while fractal boundaries are seen spread over all the chaotic sea. Noticeably, this fact leads to the large uncertainty of the final escape basin with small deviations of the initial conditions. Moreover, we note that the channel around the Lagrangian point L_1 is quite large and that 26% of total considered initial conditions belong to the larger primary basin. The spatial distribution of the escape time of the solutions of this basin is shown in Fig. 4a. We observe that many trajectories exhibit short escape time values. These solutions are spread over all the basin diagram. The trajectories that present the highest escape time are the sticky solutions locate around the stability island. By the other hand, the opening of the neck around of Lagrangian point L_2 is small and only about 14% of initial conditions analyzed belong to the exterior basin. A reasonably portion of their initial conditions appears spread over all the chaotic sea, and is associated to fractal boundaries. Analyzing the escape time for this set, as expected, the trajectories that present the lower escape time values are those whose initial conditions are in the first Poincaré cuts of the stable manifold of the Lyapunov orbit around L_2. The trajectories that present the largest escape correspond now to sparse solutions spread over all the chaotic sea.

4.2 PLUTO-CHARON SYSTEM

The Pluto-Charon system's parameter values are $\mu = 0.114730878$ and $R_H = 8.993360 \times 10^{-2}$, that is, a very high μ and a medium R_H value. In this case, 200 dtu corresponds to about 203.4 days. Figure 5 presents the Poincaré section S and the escape basin diagram for this system for $C = 3.589$. As a consequence of the mass parameter increase, the large stability region on the left side of S appears quite reduced in relation to the first case (Figs. 5a and 2a), while a noteworthy presence of stickiness effect is observable around the stability island immersed in the chaotic sea on the right side of S (Fig. 5). We note that the channel around L_1 is very large as L_2 channel opens. As R_H increases, the collisional set also expands and now presents a considerable subset interspersed with the larger primary basin and with the bounded set. As it occurs in the other two system we investigated here, the collisional set is the dominant basin for the considered initial condition set, with about 45% of the total solutions. Most solutions that belongs to this sets, presents a collisional time lower than 10 dtu, while the highest values correspond to the initial conditions associated to the fractal boundaries and stickiness effect. Analyzing Figs. 5b and 6, we note that the initial conditions of the exterior basin appear mostly in three subsets of the diagram that present smooth boundaries and correspond to the first Poincaré cuts of the stable manifold of the Lyapunov orbit around L_2. We observe an evident suppression of the fractal boundary portion of this basin in

ISSN 2176-5480

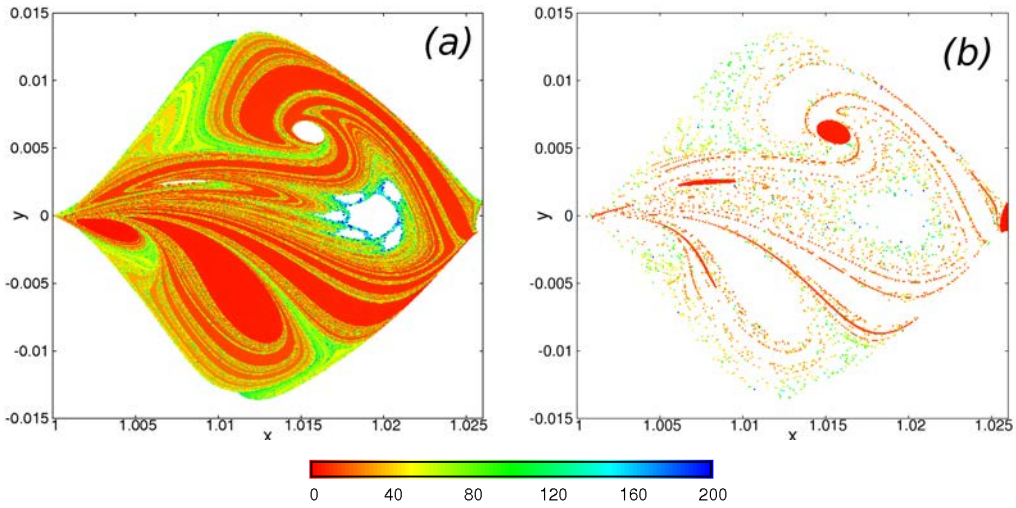

Figure 4. Escape time for Sun-Neptune system for $C = 3.005795$, for **(a)** the larger primary basin and **(b)** the exterior basin. The RGB code depicts solutions with escape time lower than 200 dtu.

relation to the first case, due to the increasing of the collisional set, i.e., trajectories that would exit the scattering region through L_2 channel with a greater escape time, collide with the primary before escaping. Contrasting with the previous case, uncertainty of final states occurs between safe escaping solutions to the larger primary region and unsafe collisional trajectories. Figure 6b shows the large region of fractal basin boundaries at the right of the diagram. Moreover, despite solutions of the larger primary basin can present escape time until 200 dtu, most part of this basin presents escape time lower than 15 dtu (Fig. 7). Remarkably, the largest escape time are again mainly around the stability island and also in the fractal boundaries regions (black dots in the Fig. 7).

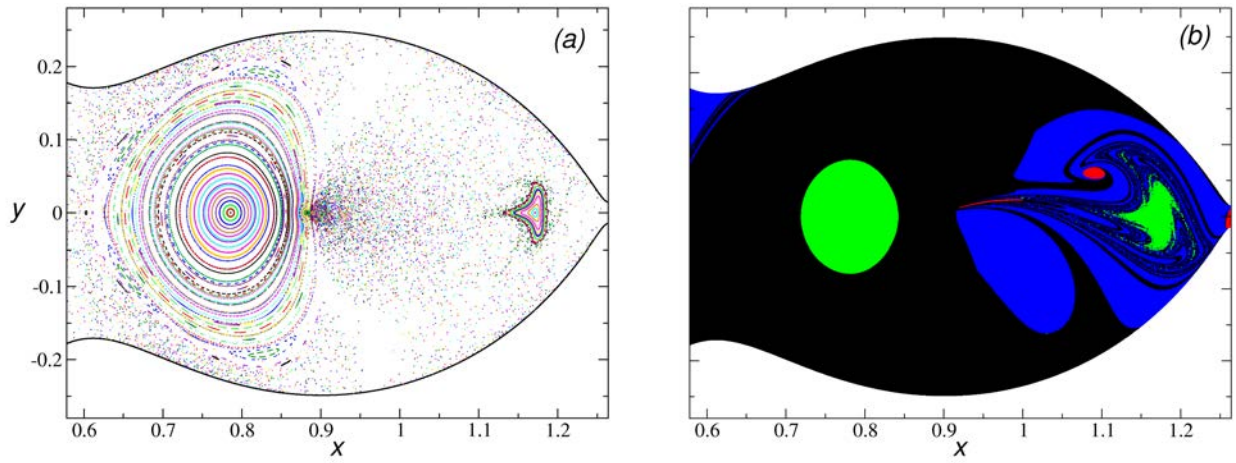

Figure 5. Results for Pluto-Charon system for $C = 3.589$. **(a)** Poincaré section S and **(b)** the escape basin diagram for $t_f = 200$ dtu, with bounded basin (green), collisional set (black), larger primary basin (blue) and exterior basin (red).

4.3 JUPITER-EUROPE SYSTEM

This third system corresponds to a case of low mass parameter combined with a high scaled primary radius. Specifically, for the Jupiter-Europe system, we have $\mu = 2.528009407 \times 10^{-5}$ and $R_H = 1.1432389 \times 10^{-1}$. We note that, indeed, this new R_H is just about 1.268 times greater the value of the second system. Moreover, this value of μ is about half of the value of the first system. Figure 8 presents the Poincaré section S along with the escape basin diagram for $C = 3.00362$. Now, 200 dtu equates 112.8 days. As well as in the first case, when the neck around the Lagrangian point L_2 opens, the neck around L_1 is still small. Particularly, stickiness effect around of the small stability island is quite negligible.

The most astonishing fact in this case is the significant growing of the collision set, corresponding to about 90% of the considered initial conditions. Despite collisions are observed until t_f, most trajectories of this set collides before 20 dtu, as illustrated by Fig. 9. The larger primary basin (3.2%) and the exterior basin (1.5%) add together approximately only

ISSN 2176-5480

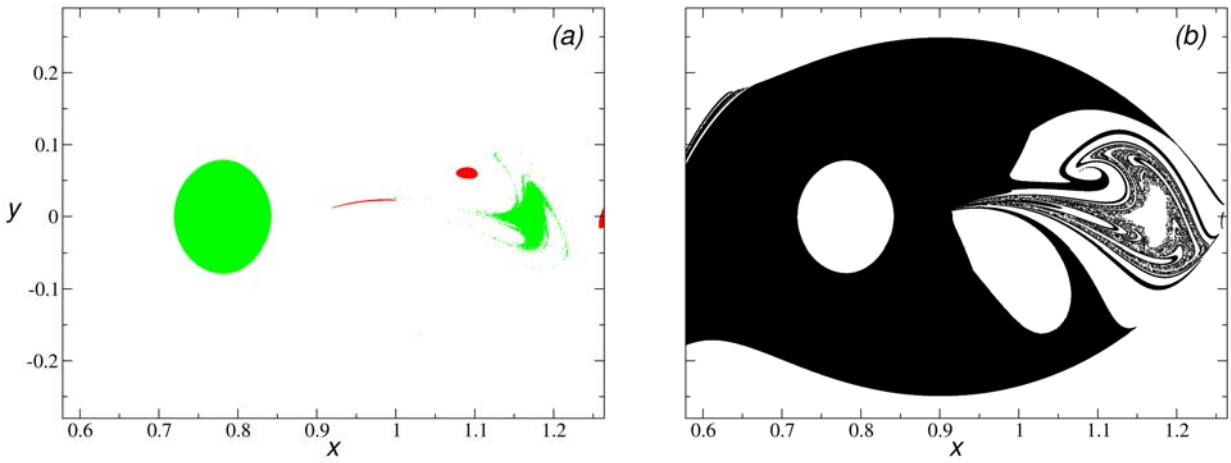

Figure 6. Detail of the escape basin diagram for Pluto-Charon system for $C = 3.589$ and $t_f = 200$ dtu, presenting **a** the bounded basin (green) and the exterior basin (red), and **b** the collisional basin (black).

4.7% of the total initial conditions analyzed. A similar amount corresponds to the bounded set. All trajectories escape from the scattering region with a time span lower than 25 dtu. Surprisingly, no solution escapes with a time span greater than 25 dtu and almost no fractality in the escape basin boundaries is observable.

Moreover, Fig. 9 presents sharp boundaries between solutions which escapes with distinct time values. How this regions of sharp boundaries are formed is also an important issue to be investigated.

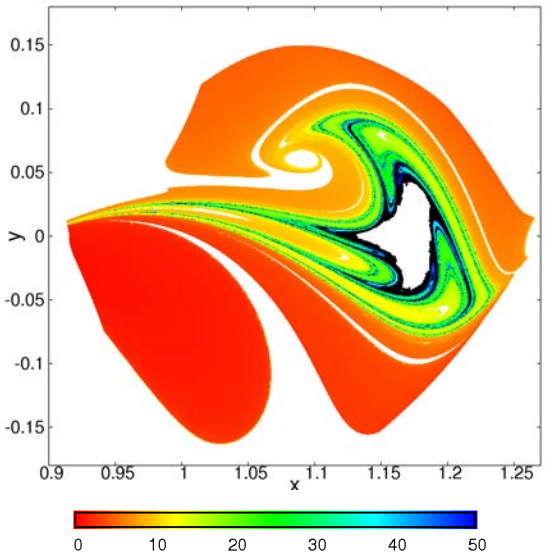

Figure 7. Escape time of the larger primary basin in the Pluto-Charon system for $C = 3.589$ and $t_f = 200$ dtu. The RGB code depicts solutions with escape time lower than 50 dtu, while black dots represents the solutions with higher values.

ISSN 2176-5480

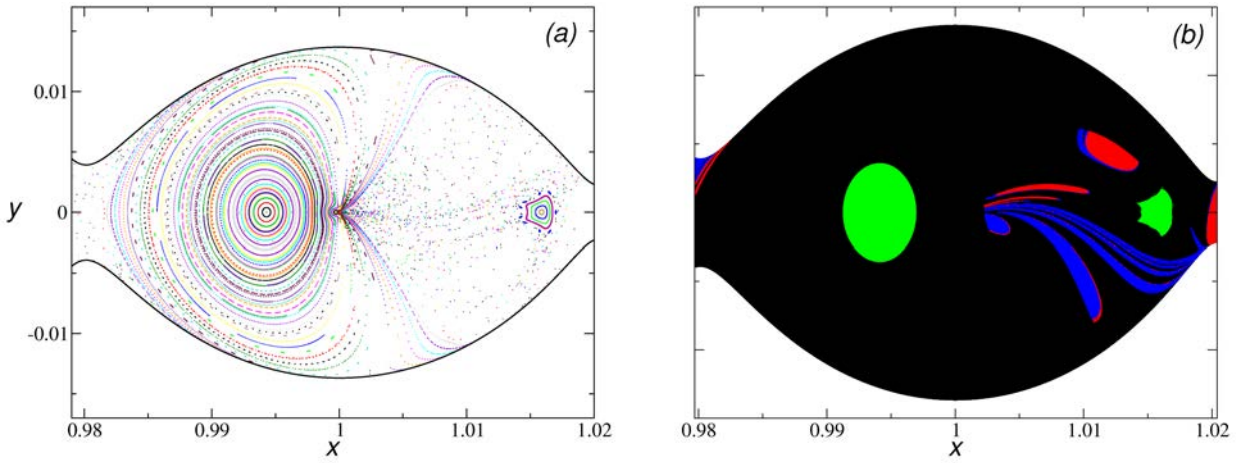

Figure 8. Results for Jupiter-Europe system for $C = 3.00362$. **(a)** Poincaré section S and **(b)** the escape basin diagram for $t_f = 200$ dtu, with bounded basin (green), collisional set (black), larger primary basin (blue) and exterior basin (red).

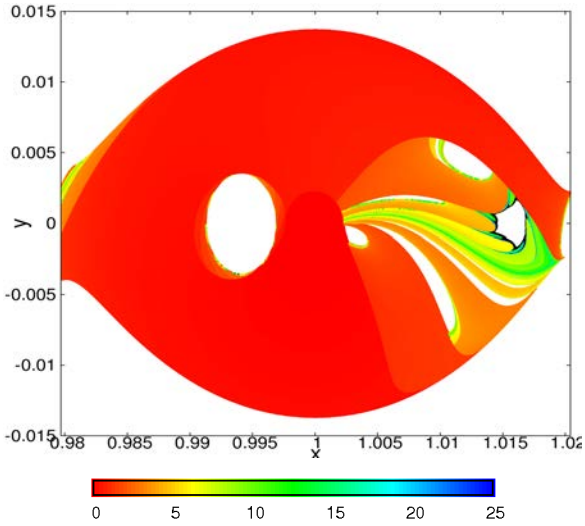

Figure 9. Collisional time in the Jupiter-Europe system for $C = 3.00362$ and $t_f = 200$ dtu. The RGB code depicts solutions with collisional time lower than 25 dtu, while black dots represents the solutions with higher values.

5. CONCLUSION

In this contribution the escape dynamics of a third body in a scattering region around the smaller primary was investigated for the planar circular restricted three-body problem. Three subsystems of the Solar system were analyzed, namely, Sun-Neptune, Pluto-Charon, and Jupiter-Europe. This variation corresponds to a biparametric analysis involving the usual mass parameter of the mathematical model and the scaled average radius of the smaller primary. Initial conditions around the primary were taken in a convenient Poincaré section. The obtained results reveal a great dependence mainly with R_H. Concerning practical applications, three distinct situations are found. In the first system, Sun-Neptune, the collisional set plays no role concerning escape process, while an intense fractality is found between the two escape basins through L_1 and L_2 for medium and long term escape solutions. In the second system, Pluto-Charon, the collisional set grows and appears interspersed with the small primary basin producing a large fractal boundary set. In the third and last system, Jupiter-Europe, the collisional set dominates the escape process and almost no fractal basin boundary is found. This preliminary analysis indicates many important issues to be considered with a deeper investigation in future contributions.

6. ACKNOWLEDGEMENTS

The first author thanks CNPq (Brazil) and the second author thanks FAPESP for the grants 2010/18692-8 and 2012/21023-6.

ISSN 2176-5480

7. REFERENCES

Aguirre, J., Viana, R.L. and Sanjuan, M.A.F., 2009. "Fractal structures in nonlinear dynamics". *Reviews of Modern Physics*, Vol. 81, pp. 333–386.

Assis, S.C. and Terra, M.O., 2013. "Escape basin analyses and fractal boundaries in the planar earth-moon system". Submitted.

Bleher, S., Grebogi, C., Ott, E. and Brown, R., 1988. "Fractal boundaries for exit in Hamiltonian dynamics". *Physical Review A*, Vol. 38, No. 2, pp. 930–938.

Contopoulos, G. and Harsoula, M., 2008. "Stickiness in chaos". *International Journal of Bifurcation and Chaos*, Vol. 18, pp. 2929–2949.

Contopoulos, G. and Harsoula, M., 2010. "Stickiness effects in chaos". *Celestial Mechanics and Dynamical Astronomy*, Vol. 107, pp. 77–92.

Davis, D.C. and Howell, K.C., 2011. "Trajectory evolution in the multi-body problem with applicstions in the saturnian system". *Acta Astronautica*, Vol. 69, pp. 1038–1049.

Davis, D.C. and Howell, K.C., 2012. "Characterization os trajectories near the smaller primary in restricted problem for aplication". *Journal of Guidance, Control and Dynamics*, Vol. 35, pp. 116–128.

Gómez, G., Koon, W.S., Lo, M.W., Marsden, J.E., Masdemont, J. and Ross, S.D., 2004. "Connecting orbits and invariant manifolds in the spatial restricted three-body problem". *Nonlinearity*, Vol. 17, pp. 1571–1606.

Koon, W.S., Lo, M.W., Marsden, J.E. and Ross, S.D., 2000. "Heteroclinic connections between periodic orbits and resonance transitions in celestial mechanics". *Chaos*, Vol. 10, pp. 427–469.

Sousa-Silva, P.A. and Terra, M.O., 2012a. "Applicability and dynamical characterization of the associated sets of the algorithmic weak stability boundary in the lunar sphere of influence". *Celestial Mechanics and Dynamical Astronomy*, Vol. 113, pp. 141–168.

Sousa-Silva, P.A. and Terra, M.O., 2012b. "Diversity and validity of stable-unstable transitions in the algorithmic weak stability boundary". *Celestial Mechanics and Dynamical Astronomy*, Vol. 113, pp. 453–478.

Szebehely, V., 1967. *Theory of Orbits*. Academic Press, New York.